THE JOURNAL OF PHYSICAL CHEMISTRY B

Article

pubs.acs.org/JPCB

Spectral and Thermal Characterization of Halogen-Bonded Novel Crystalline Oligo(*p*-bromoacetophenone formaldehyde)

Narendra Pal Singh Chauhan,*[,†] Masoud Mozafari,[‡] Rakshit Ameta,[§] Pinki B. Punjabi,[∥] and Suresh C. Ameta[§]

[†]Department of Chemistry, Bhupal Nobles Post Graduate (B.N.P.G.) College, Udaipur 313001, Rajasthan, India

[‡]Bioengineering Research Group, Department of Materials and Energy Research Center, Nanotechnology and Advanced Material, Tehran, Iran

[§]Department of Chemistry, PAHER University, Udaipur 313003, Rajasthan, India

[∥]Department of Chemistry, M. L. Sukhadia University, Udaipur 313002, Rajasthan, India

Supporting Information

ABSTRACT: A novel oligomer *p*-bromoacetophenone-formaldehyde (OPBAF) was prepared by condensation polymerization in the presence of an acid as catalyst. It was characterized by FT-IR, NMR, pyrolysis GC/MS, XRD, GPC, and TG-DTG. The crystallographic parameters and space group for hexagonal OPBAF were $a = b = 2.0810$ Å and $c = 9.2340$ Å and $P\bar{3}m1$, respectively. The degradation activation energy of the oligomer was studied by the Kissinger method. The kinetic parameters were also obtained. Halogen bonding interactions in the crystalline oligomers are identified between halogen···carbonyl and halogen···halogen. Little correlation was found in the halogen bonding motifs exhibited as a function of bromine present in this oligomer, and a unique bifurcated Br···Br/Br···O=C halogen bonding synthon was identified. This newly developed oligomer may be used as an interesting material for the development of 3D-designed structural products.

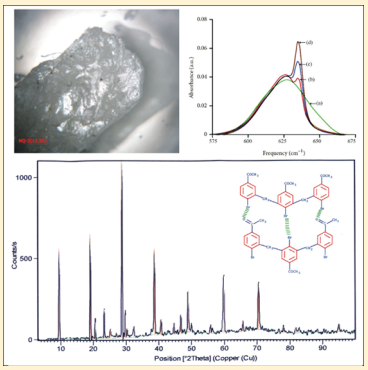

I. INTRODUCTION

It is observed that the density of electrons around the nucleus of halogen atoms is highly anisotropic in nature. Therefore, halogen atoms may take part in various intermolecular interactions. Halogen bonding is actually a noncovalent interaction between halogen atoms or a halogen atom and carbonyl group, where the halogen atom acts as an acceptor of electron density. In such a bonding, halogens act as an electrophile (Lewis acid). Halogen bonding may be represented by D···X−Y, where X is a halogen, D is the electron-donor and Y is other atom, such as carbon, halogen, nitrogen, etc.

The first report on halogen bonding was published by Guthrie[1] in 1863. The X-ray diffraction studies carried out by Hassel et al.[2,3] confirm the short intermolecular interaction between oxygen and bromine atoms present in 1,4-dioxane and liquid bromine, respectively. The strong interaction between oxygen and bromine atoms was estimated by computing the O−Br distance (2.71 Å) in the crystal system.The isolation of complexes prepared by the interaction between Lewis bases and halogen molecules is easily determined by using infrared spectroscopy. The importance of halogen bonding, analogous to hydrogen bonding, has been realized in recent times.[4] Halogen bonding is employed for the organization of radical cationic salts, fabrication of molecular conductors, and formation of liquid crystals.[5−13] Moreover, halogen bonding serves as an additional tool for the development of crystal engineering.[14−22]

Halogen bonding in porous structures is significant because these interactions are weaker than hydrogen bonding, which is probably due to the small range of pore sizes formed by close packing. Utilization of different intermolecular interactions between nitrogen heterocycles, carbonyl groups, amines, and organic halides to construct their porous structures has been reported by Pigge and co-workers.[23] In biological systems, halogen bonding has its importance as a result of their high directionality and specificity. Therefore, they can be used effectively in drug design to direct the binding of ligands to the target sites.[24] Auffinger and co-workers[25] identified the presence of halogen bonding as halogen−oxygen, halogen−nitrogen, and halogen−sulfur interactions in nucleic acid and protein−substrate complexes. The importance of halogen bonding for substrate specificity, binding, and molecular folding at the biomolecular level has been described.[26−28]

A covalently bonded atom of Groups IV−VII and a negative site can have a covalent interaction as a σ-hole bond. This negative site may be either a lone pair of a Lewis base or an anion. A region of positive electrostatic potential is involved, which is named an σ-hole, which is due to the anisotropy of distribution of the atom's charge. Halogen bonding is such a type of σ-hole interaction. It can be explained on the basis of

Received: October 13, 2014
Revised: January 11, 2015

DOI: 10.1021/jp510320g
J. Phys. Chem. B XXXX, XXX, XXX−XXX

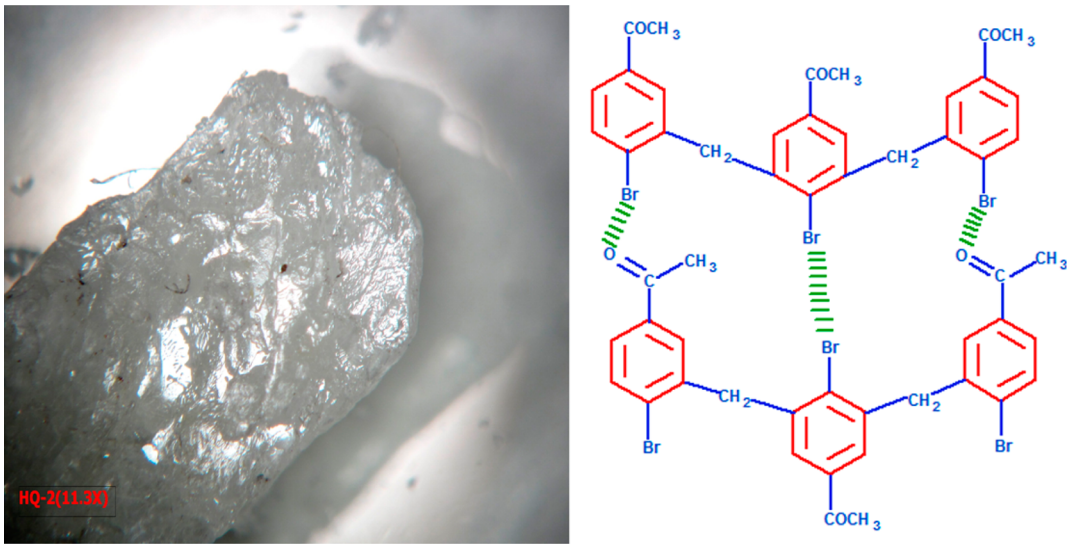

Figure 1. Proposed two-dimensional network and optical photograph of OPBAF.

electrostatics and polarization with dispersion. The strength of this interaction depends on the magnitude of electrostatic potentials (positive as well as negative) of the σ-hole and the negative site. In some cases, the polarization of the negative site reaches to the extent that it can be considered a dative sharing. The interactions of the σ-hole with the neutral bases are not thermodynamically favorable in the gas phase, which may be due to a comparatively greater entropy loss in the complex's formation.[29−34]

Halogen bonding is actually an electrostatic attraction between a positive region and a lone pair of a Lewis base. The degree of sp hybridization, polarizability of X, and the electronegativity of R reflect the presence and magnitudes of such positive potentials on some covalently bonded halogens along with the characteristic directionality of the interaction. When the strength of the halogen bonding was compared, it was found in the order as I > Br > Cl. Nowadays, halogen bonding plays an important role in designing new materials, including crystal engineering.

Recently, Esrafili[35] has investigated the nature of interactions in solid 2,6-dibromo-4-nitroaniline (DBNA) and by using symmetry-adapted perturbation theory (SAPT) analysis and concluded that the stability of Br···Br is mainly attributed to the dispersion; only a small role is due to electrostatic forces. An interesting finding was that, according to energy decomposition analysis, halogen bonds are dependent on both electrostatic and dispersion interactions. The complete understanding of the hydrogen/halogen bonding interactions was studied using the electronic structure of DBNA in the solid phase. The existence of halogen bonding within a halogenated crystalline system and within natural organic molecules is easily explained by using the above-mentioned system. This study gives very valuable information about the insight of the origin and strength of halogen bond formation and a strategy to fabricate a new kind of advanced materials for possible drug delivery applications.

High-temperature-resistant composites, photoresistant materials, thermostable materials, block copolymers, antistatic materials, adhesives, etc. may be synthesized using various oligomers. Flame-resistant composite materials such as lead-storing battery cathodes have been prepared by halogen and sulfur derivatives of oligophenols.[36]

Because of such an importance of oligomer and halogen bonding, the oligomer of *p*-bromoacetophenone and formaldehyde containing halogen bonding has been synthesized. Identification of this oilgomer (OPBAF) was done by FT-IR, FTIR-ATR, NMR, XRD, GPC, and TG-DTG. The optical photograph and proposed structure of the halogen-bonded oligomer are presented in Figure 1. The Kissinger method was used to determine the degradation activation energy and thermodynamic parameters of OPBAF. This newly synthesized material could be an exciting candidate for liquid crystal applications as a result of the presence of halogen bonding.

II. EXPERIMENTAL SECTION

II.A. Materials. *p*-Bromoacetophenone (Sisco Research Laboratories (SRL), India) was recrystallized using rectified spirit. Formaldehyde (37%) (AR grade, Merck, India) was used as received. All other chemicals, solvent, and indicators were of analytical grade (Thomas Baker, India). Doubly distilled water was used for all the experiments.

II.B. Synthesis of the Oligomeric Crystals (OPBAF). In some of our previous work, we prepared bioactive polymers by a polycondensation polymerization method in which HCl was used as a catalyst. The method and acid catalyst are common in the present work, too. The reactants, *p*-bromoacetophenone and formaldehyde, were mixed in 35 mL of ethanol. The mixture was stirred well for ∼8 h at 80 °C and then refluxed for ∼6 h. The solution was cooled and transferred to crystal growth vessels and allowed to crystallize by slow evaporation at room temperature. The synthesized compound was then dissolved in mixed tetrahydrofuran and acetone solvent (25/75 V/V) and purified by repeated crystallization (Scheme 1).

Using a slow evaporation method, the oligomer was prepared within a period of 2 weeks. A picture of one of the crystals with dimensions up to 4.9 × 1.3 × 3.8 cm^3 obtained from the mixed solvent is shown in Figure 1.

Halogen bonding involving solvents in solution phase chemistry in bulk crystals and at the monolayer level has been demonstrated theoretically and experimentally. It has been shown that halogen bonding interactions in the solid phase can also be significant in multilayer films of chelating resin moieties.[37]

DOI: 10.1021/jp510320g
J. Phys. Chem. B XXXX, XXX, XXX−XXX

Scheme 1. Synthesis of OPBAF

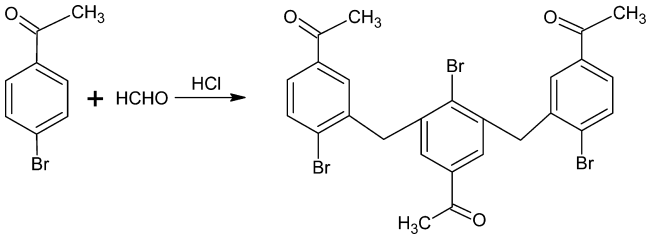

III. CHARACTERIZATION

III.A. FT-IR Analyses and Sample Preparation. The infrared spectra for identifying the functional groups and the existence of halogen bonding were recorded using a PerkinElmer 2000 FT-IR spectrometer with a horizontal attenuated total reflection (ATR) cell (USA).

The ATR diamond crystal was carefully cleaned with pure isopropyl alcohol. About 10 mg of powdered sample was carefully placed on the diamond crystal surface, and the spectrum was recorded as transmittance under 100 N. The spectrum was scanned between 3600 and 600 cm^{-1} at a resolution of 4 cm^{-1}. All experiments were carried out at room temperature, including the dilution experiments, and cyclohexane was used to record the background spectra during each dilution. A liquid sample holder with NaCl window was used, and the resolution of the FT-IR spectrometer was set at 1 cm^{-1} during each experiment.

III.B. NMR Analyses. ^{1}H and ^{13}C NMR spectra were recorded in DMSO-d_6 with Bruker DPX 400 MHz spectrometer (Germany) at a frequency of 400.13 and 100.61 MHz, respectively. The ^{1}H NMR spectrum was recorded using the standard pulse sequence given in the Bruker pulse program library. The 32 K data points were accumulated with 5 s delay times between the 16 successive scans for ^{1}H. For the ^{13}C, a total of 6000 scans containing 16 K data points were accumulated with a relaxation delay of 2 s.

III.C. GC/MS and Optical Microscopy Analysis. The qualitative and quantitative information about the synthesized OBPAF was obtained from a pyrolysis GC/MS, which consists of a GC (Autosystem XL, USA) and MS (PerkinElmer; model Turbo Mass, USA). Samples of ~100 mg were analyzed. The sample was placed into a quartz tube, which was introduced into the Pyroprobe automatically. No solvent was used, so there was no need for a solvent delay. The photograph of the oligomer in Figure 1 was taken using a Zeiss Discovery-V20 (Switzerland) optical microscope.

III.D. GPC Analysis. Gel permeation chromatography (GPC) was used to determine the average molecular weight and polydispersity index of OPBAF. It was performed with a setup consisting of a Waters 600 pump (USA) and two ultra styragel columns and equipped with a Waters differential refractometer and calibrated with the standard linear polystyrene with THF as the eluent at a flow rate of 1 mL/min.

III.E. X-ray Diffraction Analysis. The X-ray powder diffraction studies were carried out to characterize the crystallinity of the oligomer crystals using a Philips Xpert MPD diffractometer (USA) employing Cu Kα of 1.53 Å in the 2θ range 0−100 ° and 2 kW. The as-grown crystals of the title material were subjected to single crystal XRD employing Bruker Smart Apex CCD diffractometer (Germany) using Mo Kα (l = 0.7107 Å).

III.F. Thermal Analyses. Thermal degradation experiments were carried out in a Mettler-Toledo Star system, model AG-2007, TG instrument under air atmosphere over a temperature range of 30−600 °C. First, the nitrogen flow rate was at 45 mL/min, and then air was purged at 80 mL/min. The total mass of the sample taken was 6−9 mg for each run of the experiments. An alumina crucible (70 mL) was used as a sample holder. The experiments were repeated three times at a heating rate of 20 °C/min to confirm the repeatability of the experiments and authenticity of the generated data. Experiments were conducted in dynamic conditions at different heating rates of 10, 20, 30, and 40 °C/min.

IV. RESULTS AND DISCUSSION

IV.A. Spectral Analyses. The ATR spectrum of the compound (Figure 2) showed bands at 1673 cm^{-1} (C═O),

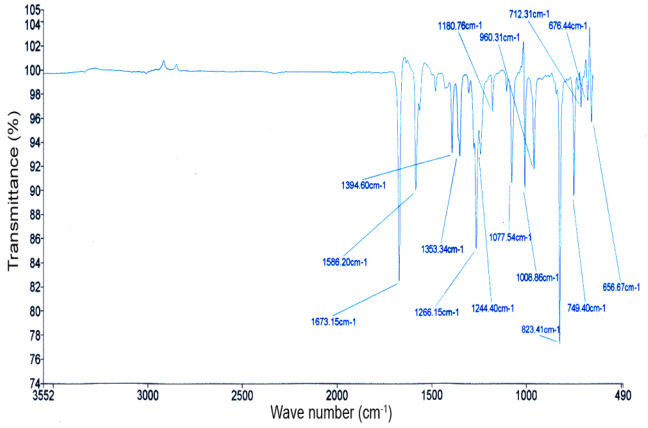

Figure 2. FT-IR (ATR) spectrum of OPBAF.

1586 and 1353 cm^{-1} (C═C stretching in aromatic ring), and 1394 cm^{-1} (CH_2 linkage) along with other bands at 1266, 1244, 1077, 1008, 749, 712, 676, and 657 cm^{-1}. The appearance of an ATR peak at 1394 cm^{-1} due to CH_2 linkage further supports the formation of product.

The halogen bond is considered as the strongest noncovalent intermolecular force, and it can be easily identified thermodynamically. It is known that the vibrational frequency shift in any hydrogen-bonded complex is proportional to the strength of that hydrogen bond.[38] Its magnitude may be correlated with complexation enthalpies. The same can be applied to the case of the halogen bond. The results obtained from FTIR give an idea about the change in enthalpy during this halogen bond formation. Because the effect of halogen bonding on C−Br stretching does not give any idea about intermolecular self-halogen bonding, therefore, some dilution experiments were carried out with some halogen bonding inactive solvents.

The intermolecular self-halogen bond can be indicated by eq 1, where one molecule utilizes its bromine atom with the oxygen atom of the other molecule.

$$(OPBAF)_A + (OPBAF)_B <=> (OPBAF)_A \cdots (OPBAF)_B \quad (1)$$

As a result of the dilution experiments, the equilibrium shows a shift toward the left that is, the self-halogen-bonded molecules will decrease, and separated molecules will increase upon

DOI: 10.1021/jp510320g
J. Phys. Chem. B XXXX, XXX, XXX−XXX

dilution, and with increasing dilution, the component at the higher frequency becomes more and more intense.

The dilution test was performed by using cyclohexane as a solvent, and the result is depicted in Figure 3. The vibration

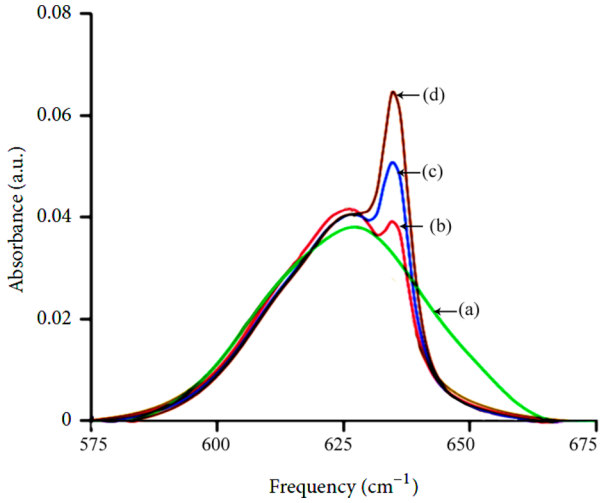

Figure 3. FT-IR absorbance of C−Br bending vibration with dilution: (a) pure oligomer and (b) 0.05, (c) 0.1, and (d) 0.15 M.

absorption at 630 cm^{-1} is for the C−Br bending vibration. This peak was broad in pure oligomer, but as the dilution increases, it is split into two components. Moreover, with an increase in the dilution, the component at the higher frequency became more intense. The results showed that the C−Br bending vibration at 630 cm^{-1} split into two components: first, at lower frequency (625 cm^{-1}), and the other, at a higher frequency (636 cm^{-1}). The lower frequency may be due to C−Br in the halogen bonding, and the higher frequency may be correlated to C−Br free of halogen bonding. It is clearly indicated by the FTIR data in Figure (2).

Intermolecular packing arrangements of different oligomer motifs can be simply explained in terms of translations along the *y*-direction (Figure 1). In addition, one oligomer can be flipped about its longitudinal molecular axis, which is along the *x*-axis, to yield a different pattern in which both the C═O···Br and Br···Br linkages can be seen. This oligomeric motif further flipped with increasing temperature. The structure of the solvation shell and movement of solvent molecules is affected by the oligomeric concentration. It was observed that with an increase in the oligomer concentration at ambient conditions, the mobility of the cyclohexane molecules was decreased. Reorientation of the molecular plane is also hindered by the oligomer, and therefore, it was found that reorientation of molecules becomes more anisotropic with the oligomer concentration. It is also reported that interactions between oligomer motifs are weaker and the reorientation of the solvent is more isotropic at elevated temperature.[39,40]

The ^{1}H NMR spectrum of the synthesized product exhibited the characteristic signals of a singlet for methyl protons at δ 2.46, a singlet for two protons of methylene at δ 3.35, and multiplet for aromatic protons in the region of δ 7.59−7.80. Appearance of a signal at δ 3.35 due to CH_2 supports the formation of oligomers between *p*-bromoacetophenone and formaldehyde. A signal due to solvent (DMSO) appeared at δ 2.50. Signals in ^{13}C NMR at 196, 127−135, 40 and 39.7, 39.5, 26.4, and 25.8 appeared to be due to the C of C═O, aromatic ring, CH_2, solvent (DMSO), CH_3, and C−Br, respectively. These signals further support the framework of the proposed structure.

IV.B. Pyrolysis GC/MS and Molecular Weight Measurements. The degradation mechanism experienced by the oligomer was free-radical processes, which were initiated by bond dissociation at the particular pyrolysis temperature. The total ion chromatogram for pyrolysis of the oligomer at 200 °C is shown in Figure 4. The peaks were identified by using the NIST library. The large peak at 16.4 min was attributed to *p*-bromoacetophenone (16.49), with a large abundance; the other relatively low intensity peak at 1.86 min was attributed to the oligomer unit without any side groups. These observed peaks strongly suggest the proposed framework of the OPBAF.

The average molecular weight of the oligomer was determined by gel permeation chromatography (Figure 5). The number-average molecular weight ($\bar{M}_n$) and weight-average molecular weight ($\bar{M}_w$) were 209.8 and 229.5,

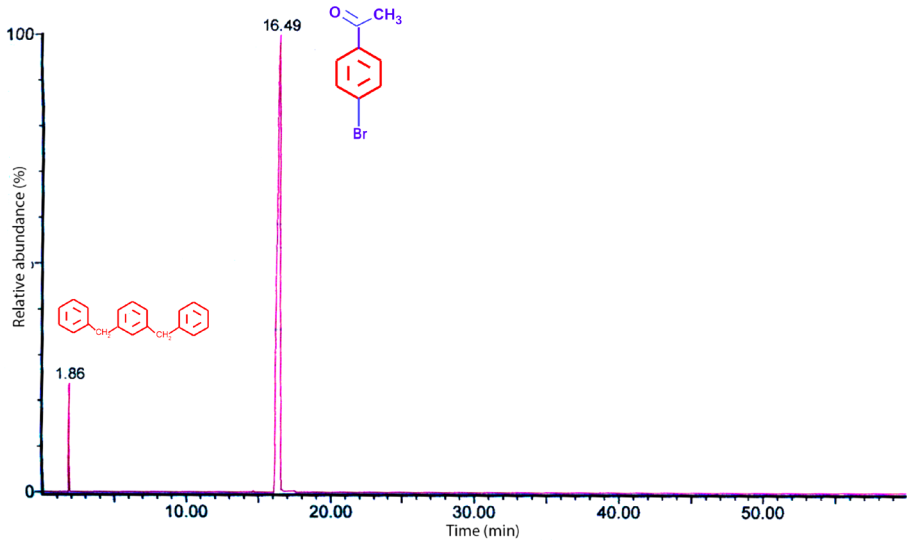

Figure 4. Pyrolysis GC/MS total ion chromatogram of OPBAF.

DOI: 10.1021/jp510320g
J. Phys. Chem. B XXXX, XXX, XXX−XXX

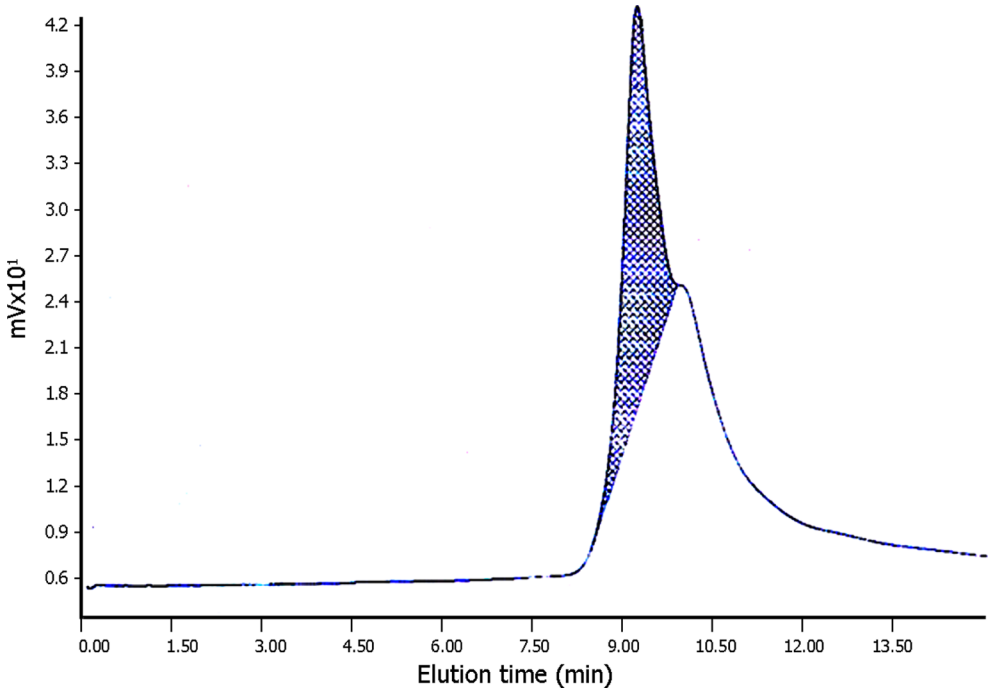

Figure 5. Size-exclusion chromatogram of OPBAF.

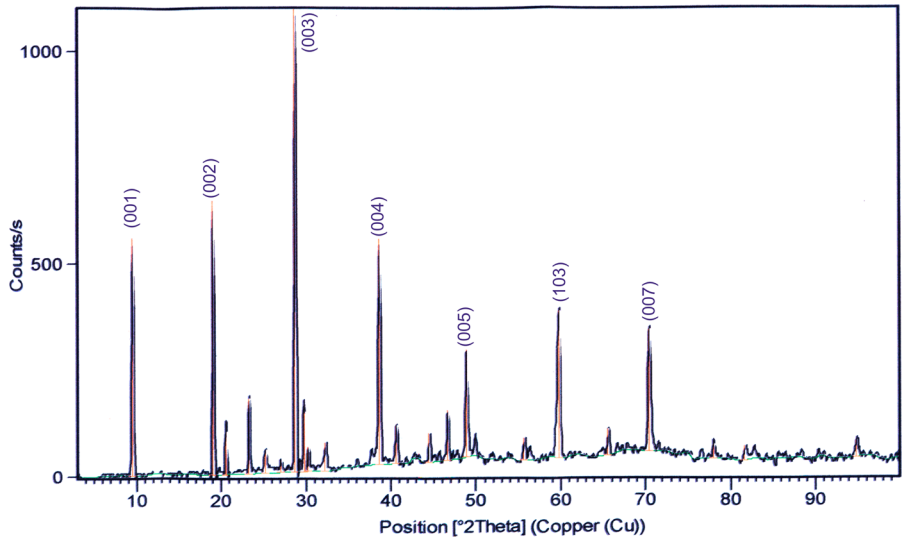

Figure 6. X-ray diffractogram of OPBAF.

respectively. The polydispersity index ($\bar{M}_w/\bar{M}_n$) was found to be 1.09. The average molecular weight ($\bar{M}_z$) was 250.

IV.C. Powder X-ray Diffraction Analysis. Powder X-ray diffraction analysis was carried out to confirm the crystallinity and also to identify the lattice parameters (Figure 6). The sample was scanned over the range 10−90°, 2θ at a rate of 2°/min. The hkl values were simulated and using the experimental d values, the lattice parameters were calculated. The XRD pattern has diffraction peaks at 2θ (relative intensity %) = 9.5° (50.4), 19.1° (58.3), 20.7° (7.7), 23.4° (13.6), 25.2° (4.8), 27.1° (2.3), 28.8° (100), 29.9° (10.8), 30.3°(3.7), 32.2° (5.1), 38.7° (47.9), 40.7° (8.1), 44.5° (5.2), 46.7° (9.2), 48.9° (22.7), 55.7°(4.1), 59.9° (26.6), 65.7° (4.8), 70.5° (29.4), 78.1° (4.8), 81.8° (4.4), and 94.9° (9.9).

The calculated unit cell parameters were a = 2.0810 Å, b = 2.0810 Å, c = 9.2340 Å, α = 90.0, β = 90.0 and γ = 120.0. These values agreed well with reported values,[41] confirming that the crystal belongs to the $P\bar{3}m1$ space group. Calculated and measured density and volume of cell were 4.50 g/cm^3, 4.54 g/cm^3 and 34.6 × 10^6 pm^3.

The crystallite size (t) based on the peak appeared at 2θ = 28.8° (fwhm =0.3444), can be calculated by using Scherrer's formula:

$$t = 0.9\lambda/\beta\cos\theta \quad (2)$$

where λ is the wavelength of X-rays used (1.5406 Å), β is the full width at half-maximum (fwhm) and θ is the angle of diffraction. The average crystallite size of the prepared nanopowder was found to be 0.42 nm which is in the order of nanoscale.

IV.D. Thermal Analysis. The thermal stability of the OPBAF crystals was identified by thermogravimetry (TG) and

DOI: 10.1021/jp510320g
J. Phys. Chem. B XXXX, XXX, XXX−XXX

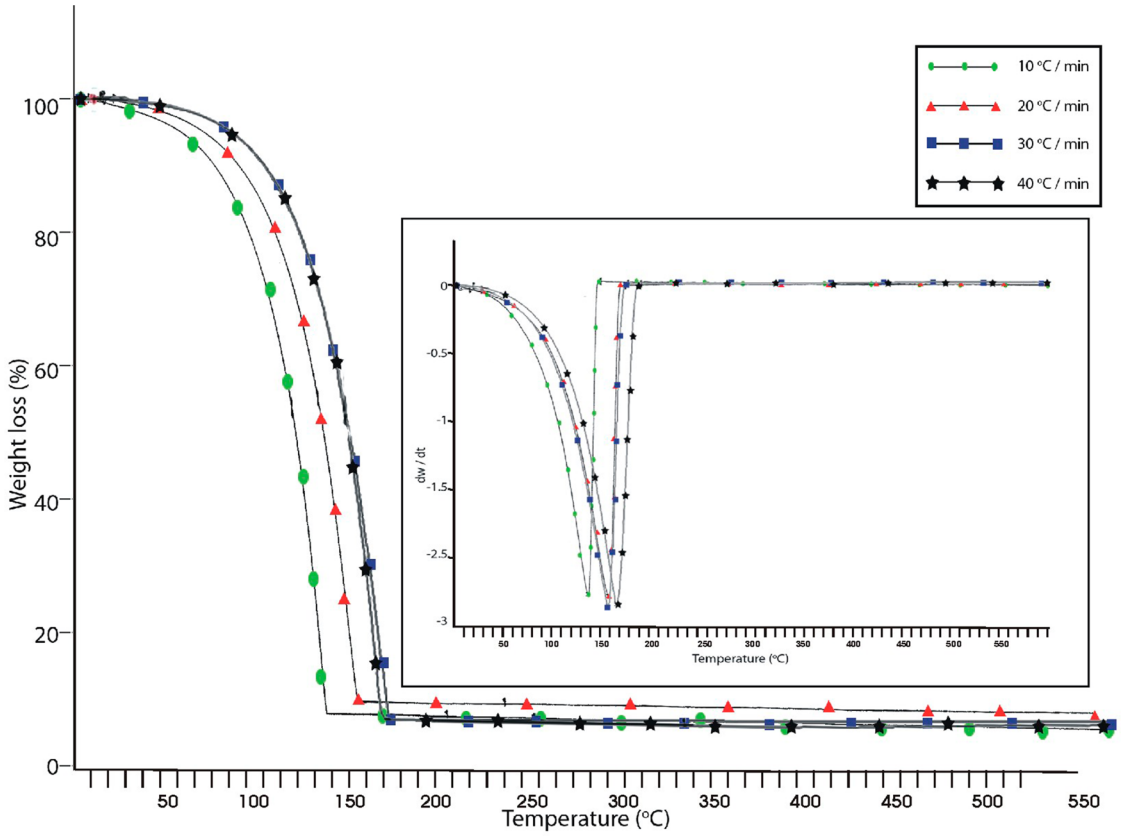

Figure 7. TG -DTG plots of OPBAF obtained in nitrogen atmosphere at different heating rates.

derivative of thermogravimetry (DTG). To find activation energy during degradation of the oligomer, TG-DTG analyses at different heating rates were carried out in a nitrogen atmosphere. The TG-DTG at different heating rates (10, 20, 30, and 40 °C/min) is shown in the inset in Figure 7. The onset, endset and decomposition temperature are tabulated in Table 1. The TG-DTG curve shows that the material is stable up to 124.8 °C. It shows only one stage degradation and there is no phase transition occurred before the melting point. After the occurrence of a step of weight loss at 75−150 °C, the weight loss remained almost constant. This stage of degradation is probably due to side group elimination, like −Br, and $-COCH_3$ in the form of HBr, carbon monoxide and carbon dioxide. Thus, the formation of OPBAF was confirmed from TG-DTG analysis.

Table 1. TG-DTG data from different heating rates for oligomer, OPBAF

heating rate (°C/min)	$T_{onset} - T_{endset}$	decomp temp (T_d)	activation energy (kJ/mol)
10	124.8−170.5	165.4	9.34
20	138−191.2	182.1	
30	145.5−199.8	188.1	
40	154−210.5	195.5	

The activation energy, E_a, during thermal degradation was computed by the Kissinger method.[42−47] The Kissinger equation is

$$-\frac{\beta}{T_d^2} = -\ln\frac{AR}{E_a} + \frac{1}{T_d}\frac{E_a}{R} \quad (3)$$

where β is heating rate; T_d, the decomposition temperature; R, the gas constant; and E_a, the activation energy.

A and E_a were obtained by plotting $-\ln(\beta/T_d^2)$ versus $1/T_d$, where T_d is the peak decomposition temperature.

Thermodynamic Parameters. By using data of TG-DTG analyses at 10 °C/min using the Kissinger method, thermodynamic parameters such as apparent entopy change (ΔS^*), free energy of activation (G^*), and reaction rate of activation (k_r) have been determined on the basis of thermal activation energy using the equations given below. Entropy of activation (ΔS^*):

$$\Delta S^* = 2.303R \log\frac{Zh}{kT_d} \quad (4)$$

where k is the Boltzmann constant, h is the Planck constant, and T_d is the peak temperature from DTG.

Free energy of activation (G^*):

$$G^* = E^* - T\Delta S^* \quad (5)$$

Reaction rate constant for activation (k_r):

$$k_r = Ze^{-E^*/RT_d} \quad (6)$$

By using data of thermogravimetric analysis, thermodynamic parameters such as the apparent entropy change (ΔS^*), the free energy of activation (G^*) and reaction rate of activation (k_r) were found to be 11.7 J, and 21.2 kJ/mol, and 2.2×10^{-3} min^{-1}, respectively. The positive value of ΔS^* indicates that the activated complex has a less-ordered structure than the crystal system having halogen bonding.

DOI: 10.1021/jp510320g
J. Phys. Chem. B XXXX, XXX, XXX−XXX

V. CONCLUSIONS

A novel method of oligomerization by condensing *p*-bromoacetophenone and formaldehyde in the presence of an acid has been presented. FT-IR and FT-IR (ATR) revealed that solid state halogen bonding was present between the oligomeric crystallites. It was further characterized by ^{1}H NMR, ^{13}C NMR, Py GC/MS, GPC, XRD, and TG-DTG. The interactions were between Br···Br and C═O···Br, where the oxygen atom of the carbonyl acted as the electron donor and the Br atom of other oligomeric molecule acted as the electron acceptor, resulting in a two-dimensional network, have been identified by dilution experiment. Flipping of two oligomeric chains greatly depends on the temperature of the oligomeric sample and also on the dynamic of cyclohexane as the solvent. The activation energy and thermodynamic parameters, including apparent entropy, free energy of activation, and reaction rate of activation during thermal degradation, also suggested intermolecular packing arrangements. This work will likely have an impact on a range of applications across diverse fields, where halogen bonding in thin films and nucleation chemistry are important.

■ ASSOCIATED CONTENT

Ⓢ Supporting Information

^{1}H NMR and ^{13}C NMR spectra and plot of $-(\ln \beta/T_d^2)$ versus $1000/T_d$ of OPBAF(Kissinger method). This material is available free of charge via the Internet at http://pubs.acs.org.

■ AUTHOR INFORMATION

Corresponding Author

*Tel. +919828306025. E-mail: narendrapalsingh14@gmail.com.

Notes

The authors declare no competing financial interest.

■ ACKNOWLEDGMENTS

Dr. Narendra Pal Singh Chauhan is thankful to his parents Ashu Singh Ji Chauhan and Aman Kunwar Rathore for encouragement.

■ REFERENCES

(1) Guthrie, M. On the Iodide of Iodammonium. *J. Chem. Soc.* **1863**, *16*, 239−244.
(2) Hassel, O.; Hvoslef, J.; Vihovde, E.; Hadler, S.; Andreas, N. The Structure of Bromine 1,4- Dioxanate. *Acta Chem. Scand.* **1954**, *8*, 873−873.
(3) Hassel, O. Structural Aspects of Interatomic Charge-Transfer Bonding. *Science* **1970**, *170*, 497−502.
(4) Metrangolo, P.; Resnati, G. *Halogen Bonding: Fundamentals and Applications*; Springer: New York, 2008, *126*, pp 1−16.
(5) Metrangolo, P.; Giuseppe, R.; Tullio, P.; Rosalba, L.; Franck, M. Engineering Functional Materials by Halogen Bonding. *J. Polym. Sci., Part A: Polym. Chem.* **2007**, *45*, 1−15.
(6) Bruce, D. W. Materials Chemistry of Alkoxystilbazoles and Their Metal Complexes. *Adv. Inorg. Chem.* **2001**, *52*, 151−159.
(7) Weingarth, M.; Raouafi, N.; Jouvelet, B.; Duma, L.; Bodenhausen, G.; Boujlel, K.; Scöllhorn, B.; Tekley, P. Revealing Molecular Self-Assembly and Geometry of Non-Covalent Halogen Bonding by Solid-State NMR Spectroscopy. *Chem. Commun.* **2008**, *45*, 5981−5983.
(8) Nguyen, H. L.; Horton, P. N.; Hursthouse, M. B.; Legon, A. C.; Bruce, D. W. Halogen bonding: A New Interaction for Liquid Crystal Formation. *J. Am. Chem. Soc.* **2004**, *126*, 16−17.
(9) Metrangolo, P.; Präsang, C.; Resnati, G.; Liantonio, R.; Whitwood, A. C.; Bruce, D. W. Fluorinated Liquid Crystals by Halogen Bonding. *Chem. Commun.* **2006**, 3290−3292.
(10) Bruce, D. W.; Metrangolo, P.; Meyer, F.; Präsang, C.; Resnati, G.; Whitwood, A. C. Mesogenic, Trimeric, Halogen-bonded Complexes from Alkoxystilbazoles and 1,4-Diiodotetrafluorobenzene. *New J. Chem.* **2008**, *32*, 477−482.
(11) Präsang, C.; Whitwood, A. C.; Bruce, D. W. Spontaneous Symmetry-Breaking in Halogen-Bonded, Bent-Core Liquid Crystals: Observation of a Chemically Driven Iso-N-N* Phase Sequence. *Chem. Commun.* **2008**, *18*, 2137−2139.
(12) Präsang, C.; Nguyen, H. L.; Horton, P. N.; Whitwood, A. C.; Bruce, D. W. Trimeric Liquid Crystals Assembled Using both Hydrogen and Halogen Bonding. *Chem. Commun.* **2008**, *46*, 6164−6166.
(13) Bruce, D. W.; Metrangolo, P.; Meyer, F.; Pilati, T.; Präsang, C.; Resnati, G.; Terraneo, G.; Wainwright, S. G.; Whitwood, A. C. Structure−Function Relationships in Liquid-Crystalline Halogen-Bonded Complexes. *Chem.—Eur. J.* **2010**, *16*, 9511−9524.
(14) Pierangelo, M.; Giuseppe, R.; Tullio, P.; Giancarlo, T.; Serena, B. Anion Coordination and Anion-Templated Assembly under Halogen Bonding Control. *CrystEngComm* **2009**, *11*, 1187−1196.
(15) Stephens, S. L.; Walker, N. R.; Legon, A. C. Molecular Geometries of H_2S ···ICF_3 and H_2O···ICF_3 Characterised by Broadband Rotational Spectroscopy. *Phys. Chem. Chem. Phys.* **2011**, *13*, 21093−21103.
(16) Stephens, S. L.; Walker, N. R.; Legon, A. C. Internal Rotation and Halogen Bonds in CF_3I···NH_3 and CF_3I···$N(CH_3)_3$ Probed by Broadband Rotational Spectroscopy. *Phys. Chem. Chem. Phys.* **2011**, *13*, 20736−20744.
(17) Stephens, S. L.; Walker, N. R.; Legon, A. C. Rotational spectra and properties of complexes $BICF_3$ (B = Kr or CO) and a Comparison of the Efficacy of ICl and ICF_3 as Iodine Donors in Halogen Bond Formation. *J. Chem. Phys.* **2011**, *135*, 224309.
(18) Thomas, N. W.; Desiraju, G. R. An Investigation into the Role of Chloro-Substituents in Hydrogen-Bonded Crystals: The Crystal Structures of the Dichlorophenols. *Chem. Phys. Lett.* **1984**, *110*, 99−102.
(19) Desiraju, G. R.; Parthasarathy, R. The Nature of Halogen··· Halogen Interactions: Are Short Halogen Contacts Due to Specific Attractive Forces or Due to Close Packing of Nonspherical Atoms? *J. Am. Chem. Soc.* **1989**, *111*, 8725−8726.
(20) Dey, A.; Desiraju, G. R. Supramolecular Equivalence of Ethynyl, Chloro, Bromo and Iodo Groups. A Comparison of the Crystal Structures of Some 4-Phenoxyanilines. *CrystEngComm* **2004**, *6*, 642−646.
(21) Reddy, C. M.; Kirchner, M. T.; Gundakaram, R. C.; Padmanabhan, K. A.; Desiraju, G. R. Isostructurality, Polymorphism and Mechanical Properties of Some Hexahalogenated Benzenes: The Nature of Halogen···Halogen Interactions. *Chem.—Eur. J.* **2006**, *12*, 2222−2234.
(22) Bui, T. T. T.; Dahaoui, S.; Lecomte, C.; Desiraju, G. R.; Espinosa, E. The Nature of Halogen···Halogen Interactions: A Model Derived from Experimental Charge-Density Analysis. *Angew. Chem., Int. Ed.* **2009**, *48*, 3838−3841.
(23) Pigge, F. C.; Vangala, V. R.; Kapadia, P. K.; Swenson, D. C.; Rath, N. P. Hexagonal Crystalline Inclusion Complexes of 4-Iodophenoxy Trimesoate. *Chem. Commun.* **2008**, *38*, 4726−4728.
(24) Lu, Y.; Shi, T.; Wang, Y.; Yang, H.; Yan, X.; Luo, X.; Jiang, H.; Zhu, W. Halogen Bonding—A Novel Interaction for Rational Drug Design? *J. Med. Chem.* **2009**, *52*, 2854−2862.
(25) Auffinger, P.; Hays, F. A.; Westhof, E.; Ho, P. S. Halogen Bonds in Biological Molecules. *Proc. Natl. Acad. Sci. U.S.A.* **2004**, *101*, 16789−16794.
(26) Steinrauf, L. K.; Hamilton, J. A.; Braden, B. C.; Murrell, J. R.; Benson, M. D. X-Ray Crystal Structure of the Ala-109 → Thr Variant of Human Transthyretin Which Produces Euthyroid Hyperthyroxinemia. *J. Biol. Chem.* **1993**, *268*, 2425−2430.
(27) Howard, E. I.; Sanishvili, R.; Cachau, R. E.; Mitschler, A.; Chevrier, B.; Barth, P.; Lamour, V.; Van Zandt, M.; Sibley, E.; Bon, C.; et al. Ultrahigh Resolution Drug Design I: Details of Interactions in

DOI: 10.1021/jp510320g
J. Phys. Chem. B XXXX, XXX, XXX−XXX

Human Aldose Reductase-Inhibitor Complex at 0.66 A. *Proteins: Struct. Funct. Bioinf.* **2004**, *55*, 792−804.
(28) Yabe-Nishimura, C. Aldose Reductase in Glucose Toxicity: A Potential Target for the Prevention of Diabetic Complications. *Pharmacol. Rev.* **1998**, *50*, 21−33.
(29) Politzer, P.; Murray, J. S.; Clark, T. Halogen Bonding and Other σ-Hole Interactions: A Perspective. *Phys. Chem. Chem. Phys.* **2013**, *15*, 11178−11189.
(30) Clark, T. σ-hole. *WIREs Comput. Mol. Sci.* **2013**, *3*, 13−20.
(31) Clark, T.; Hennemann, M.; Murray, J. S.; Politizer, P. Halogen Bonding: The Sigma-Hole. *J. Mol. Model.* **2007**, *13*, 291−296.
(32) Clark, T.; Murray, J. S.; Politzer, P. Role of Polarization in Halogen Bonds. *Aust. J. Chem.* **2013**, *67*, 451−456.
(33) Nourmohammadzadeh, M.; Lo, J. F.; Bochenek, M.; Mendoza-Elias, J.; Wang, Q.; Li, Z.; Zeng, L.; Qi, M.; Eddington, D. T.; Oberholzer, J.; Wang, Y. Microfluidic Array with Integrated Oxygenation Control for Real-Time Live-Cell Imaging: Effect of Hypoxia on Physiology of Microencapsulated Pancreatic Islets. *Anal. Chem.* **2013**, *85*, 11240−11249.
(34) Nourmohammadzadeh, M.; Rahnama, M.; Jafari, S.; Akhgar, A. R. Microchannel Flow Simulation in Transition Regime Using Lattice Boltzmann Method. *Proc. Inst. Mech. Eng., Part C* **2012**, *226*, 552−562.
(35) Esrafili, M. D. A Theoretical Investigation of the Characteristics of Hydrogen/Halogen Bonding Interactions in Dibromo-Nitroaniline. *J. Mol. Model.* **2013**, *19*, 1417−1427.
(36) Sahni, S. K.; Reedijk, J. Coordination Chemistry of Chelating Resins and Ion Exchangers. *J. Coord. Chem. Rev.* **1984**, *59*, 1−139.
(37) Gushchin, P.; Starov, G.; Haukka, M.; Kuznetsov, M.; Eremenko, I.; Kukushkin, V. Chloride−Chloroform Clusters Exhibiting Weak Hydrogen and Halogen Bondings Are Fully Characterized in the Solid State by X-ray Diffraction. *Cryst. Growth Des.* **2010**, *10*, 4839−4846.
(38) Laurence, C.; Queignec-Cabanetos, M.; Dziembowska, T.; Queignec, R.; Wojtkowiak, B. 1-Iodoacetylenes. 1. Spectroscopic Evidence of Their Complexes with Lewis Bases. A Spectroscopic Scale of Soft Basicity. *J. Am. Chem. Soc.* **1981**, *103*, 2567−2573.
(39) Muller-Plathe, F. Microscopic Dynamics in Water-Swollen Polyvinyl alcohol. *J. Chem. Phys.* **1998**, *108*, 8252−8263.
(40) Shen, T.; Langan, P.; French, A. D.; Johnson, G. P.; Gnankaran, S. Conformational; Flexibility of Soluble Cellulose Oligomers: Chain Length and Temperature Dependence. *J. Am. Chem. Soc.* **2009**, *131*, 14786−14794.
(41) Juza, R.; Friedrichsen, H. Z. Die Kristallstruktur von β-ZrNCl und β-ZrNCl. *Anorg. Allg. Chem.* **1964**, *332*, 173−178.
(42) Chauhan, N. P. S.; Ameta, S. C. Preparation and Thermal Studies of Self-Crosslinked Terpolymer Derived from 4-Acetylpyridine Oxime, Formaldehyde and Acetophenone. *Polym. Degrad. Stab.* **2011**, *96*, 1420−1429.
(43) Chauhan, N. P. S. Structural and Thermal Characterization of Macro-branched Functional Terpolymer Containing 8-Hydroxyquinoline Moieties with Enhancing Biocidal Properties. *J. Ind. Eng. Chem.* **2013**, *19*, 1014−1023.
(44) Chauhan, N. P. S. Terpolymerization of *p*-Acetylpyridine Oxime, *p*-Methylacetophenone and Formaldehyde, and Its Thermal Studies. *J. Therm. Anal. Calorim.* **2012**, *110*, 1377−1388.
(45) Chauhan, N. P. S. Spectral and Thermal Investigation of Designed Terpolymers Bearing *p*-Acetylpyridine Oxime Moieties Having Excellent Antimicrobial Properties. *Des. Monomers Polym.* **2013**, *16*, 543−555.
(46) Chauhan, N. P. S. Isoconversional Curing and Degradation Kinetics Study of Self-Assembled Thermo-Responsive Resin System Bearing Oxime and Iminium Groups. *J. Macromol. Sci., Part A: Pure Appl. Chem.* **2012**, *49*, 706−719.
(47) Chauhan, N. P. S. Preparation and Characterization of Bio-Based Terpolymer Derived from Vanillin Oxime, Formaldehyde and *p*-Hydroxyacetophenone. *Des. Monomers Polym.* **2014**, *17*, 176−185.

DOI: 10.1021/jp510320g
J. Phys. Chem. B XXXX, XXX, XXX−XXX